A Liquid Jet Impinging onto Rotating Convex Superhydrophobic and Hydrophilic Surfaces: Reflection or Deflection?

A. Kibar

Department of Mechanical and Material Technologies, Kocaeli University, Uzuncitlik Nuh Cimento Campus, 41180, Kocaeli, Turkey

Email: alikibar@kocaeli.edu.tr

ABSTRACT

A liquid jet impinging on stationary and rotating superhydrophobic and hydrophilic convex surfaces is experimentally investigated. The effects of the rotation and wettability of the surface and the inertia and impingement rate of the jet on the flow, and the reflection and deflection behavior of the impinging jet are examined. This study examines the effect of air film formation at the constantly regenerating interface between a superhydrophobic surface and a liquid jet. For this purpose, two copper pipes and one plexiglass pipe, which had outer diameters of 8, 22, and 50 mm, were used for the convex surfaces. The copper pipes were coated with a superhydrophobic coating with a 157° apparent contact angle. The uncoated plexiglass pipe had a 73° apparent contact angle. The Reynolds and Weber numbers ranged from 1082 to 3443 and from 3.90 to 35.12, respectively. The liquid jet was sent to the rotating convex surfaces at different impingement rates. The experimental results show that the impinging liquid jet is reflected off the stationary superhydrophobic surface. This reflection behavior is not nearly distributed from the rotation of the superhydrophobic convex surface. The distribution increases slightly with an increase in the Reynolds or Weber numbers, the diameter of the convex surface, and the impingement rate. Nevertheless, the impingement liquid jet is deflected off the stationary hydrophilic surface. This deflection increases considerably with the rotation of the convex surface. The renewal of the air film between the superhydrophobic surface and the liquid significantly reduces the viscous drag force. Therefore, the impinging liquid jet cannot be dragged by the rotating superhydrophobic convex surface.

Keywords: Superhydrophobicity; Liquid jet; Reflection jet; Liquid solid interface; Wettability; Jet impingement.

1 INTRODUCTION

The use and applications of superhydrophobic surfaces increase daily due to their extraordinary properties. Due to the low surface energies water droplets are close to spherical on these with a high contact angle. There are two different types of superhydrophobic surfaces: Wenzel and Cassie-Baxter. For the Wenzel type, the liquid penetrates the cavities on a rough surface, and the contact angle hysteresis becomes large. These surfaces have the "rose-petal" effect. For the Cassie-Baxter type, the liquid does not penetrate the cavities and air gaps (pockets) occur between the liquid and the surface. Therefore, the water droplet rolls over the surface with small external forces (such as wind or a low tilt angle) since the contact angle hysteresis is low.

While the water drop rolls, it collects dirt particles and cleans the surface (Latthe *et al*. 2019). With

these features, both surfaces have been used in different industries and applications, such as self-cleaning, anti-icing/fogging, and drag reduction (Bhushan and Jung, 2011; Varshney and Mohapatra, 2018; Wu *et al*. 2018). Alternatively, the impingement of a liquid jet on solid surfaces is used in various industrial applications and processes such as cleaning, cooling, coating, and ink-jet printing (Landel and Wilson 2021; Lu *et al*. 2020; Zhang *et al*. 2015). In these applications, the solid surfaces are stationary, in linear motion, or rotating. When a vertical or oblique liquid jet impinges on a horizontal hydrophilic surface, the liquid spreads out as a thin film. Then, its thickness abruptly increases. The phenomena of vertical and oblique jet impingement on the horizontal hydrophilic surface are called circular (Craik *et al*. 1981) and non-circular hydraulic jump, respectively (Abdelaziz and Khayat 2022; Kate *et al*. 2007).

The liquid jet impinging on the solid surface has different behaviors, depending on several factors such as the Reynolds (Re) or Weber (We) number of the jet and the contact angle of the solid surface. The wettability of the surface plays a significant role in the behavior of the liquid jet impinging on the solid surface. The spreading behavior of an impinging liquid jet on a non-wetting surface has been classified by Kibar *et al*. (2010) as braiding, spreading, splashing, and reflection flows. The orthogonal liquid jet that impinges on a horizontal superhydrophobic surface does not continue as a jet after spreading as a thin film on the surface; and then, it breaks up into liquid droplets (Prince *et al*. 2015; Sen *et al*. 2019). When a liquid jet impinges on a superhydrophobic surface obliquely, it gains the stored surface energy depending on the large free surface area compared to the spreading (wetted) area (Kibar 2016). The energy for the spreading and reflection behavior of an obliquely impinging liquid jet onto vertical surfaces has been defined by Kibar, (2016). The contact angle (90<θ<150°), an indicator of the free surface energy, is lower on the hydrophobic surface than on the superhydrophobic surface (θ>150°) (Erbil *et al*. 2003). Therefore the impinging liquid jet gains the low stored surface energy from the hydrophobic surface, resulting in braiding flow over the surface instead of reflection flow (Kibar *et al*. 2010; Mertens *et al*. 2005).

Li *et al*. (2021) and Yang *et al*. (2020) have investigated the spreading behavior of a liquid jet impinging the non-wetting surface at a given angle of inclination with a comprehensive theoretical analysis. They have stated that the spreading size of the impinging liquid jet could be affected by the wettability of the surface. Cardin *et al*. (2021) have investigated the rebound of the obliquely impinging large liquid jet from the superhydrophobic surface. They developed a simple prediction model to define the flow dimensions of a spreading liquid jet.

The surface energy of the liquid-gas, liquid-solid, and solid-gas interfaces can be expressed as Eq. (1) (Yao *et al*. 2021). This energy can be considered the potential energy of a spreading droplet or an impinging liquid jet on a hydrophobic or superhydrophobic surface.

$$E_{\gamma_{LG}} = A_{LG}\gamma_{LG}, \quad E_{\gamma_{LS}} = A_{LS}\gamma_{LS},$$
$$E_{\gamma_{LG}} = A_{GS}\gamma_{GS} \tag{1}$$

where A_{LG} and A_{LS} are the surface areas between the liquid and the gas and the spreading area between the liquid and the solid, respectively, and γ_{LG}, γ_{LS}, and γ_{GS} are the surface tensions between the liquid-gas, liquid-solid and gas-solid interfaces, respectively.

The stored surface energy ($E\gamma$) can be defined as Eq. (2) (Kibar 2016; Shi *et al*. 2018).

$$E_{\gamma} = A_{LG}\gamma_{LG} + A_{LS}(\gamma_{LS} - \gamma_{GS}) \tag{2}$$

The surface energy equation of the spreading liquid (Eq. (2)) can be simplified using Young's equation (Eq. (3)). Thus, Eq. (4) is obtained as a definition of the stored surface energy.

$$\gamma_{LS} - \gamma_{GS} + \gamma_{LG} \cos \theta_E = 0 \tag{3}$$

$$E_{\gamma} = \gamma_{LG}[A_{LG} - (A_{LS} \cos \theta_E)] \tag{4}$$

where θ_E is the apparent contact angle of the solid surface. The contact angle is the dominant parameter in the magnitudes of A_{LS} and A_{LG}. Therefore, the contact angle of the surface dominates the stored surface energy.

The spreading inertia of a liquid jet on a surface is determined by the viscosity and surface tension of the liquid during the spreading process (Kibar 2017). Therefore, the dimensionless numbers governing the flow are the Reynolds (Eq. (5)) and Weber numbers (Eq. (6)), which are the ratios of inertia force to the viscous force and the surface tension forces, respectively.

$$Re = \frac{\rho v_{jet} d}{\mu} \tag{5}$$

$$We = \frac{\rho v_{jet}^2 d}{\gamma} \tag{6}$$

where ρ, v_{jet}, d, μ, and γ are the density of the liquid, the velocity of the liquid jet, the diameter of the jet, liquid viscosity, and the surface tension of the liquid, respectively.

From Eq. (4), the stored surface energy of the spreading liquid is affected by four variables: the surface tension, the spreading and the free surface area of the liquid, and the contact angle of the surface. The contact angle of the solid surface primarily affects the dimensions of the free surface, such as spreading and free surface area. An impinging liquid jet on a superhydrophobic surface at an angle cannot spread over a wide area because it has low free surface energy due to the surface tension of the liquid. Therefore, the capillary force of the liquid jet, which is the sum of the Laplace pressure and the surface tension forces that depend on the curvature of the liquid, prevents the liquid from advancing along the three-phase contact line (TPCL) (Chatterjee and Flury 2013; Kibar 2017). Consequently, the spreading liquid, which has a large stored surface energy, reflects off the superhydrophobic surface. The stored surface energy is converted into kinetic energy, resulting in the reflection of the liquid from the surface (Kibar 2016; Satpathi *et al*. 2021).

The motion of the contact line is determined by the dynamics of the molecules within a three-phase contact line, where the solid, liquid, and gas phases meet (Blake 2006; Eral *et al*. 2013; Linder *et al*. 2015). The three-phase contact line is effective in spreading the liquid on the surface than the spreading area. The motion of three-phase contact line is directly related to the contact angle and the contact angle hysteresis (Kibar 2017). Kibar (2018b) has studied the spreading profiles of impinging liquid jets on a non-wetting surface. The widest widths and spreading profiles at the TPCL were predicted in this study. De la Cruz and Mäkiharju (2022) have studied the liquid patch topology that occurs when a liquid jet with varying hydrophobicity impinges on the

underside of a flat plate. They compared their data with the results from several previous studies. They determined that the wettability of the surface was a key parameter, and the momentum loss and wetted area increased with an increase in the contact angle of the surface.

Kibar (2017) has experimentally and numerically examined the impingement of a liquid jet on hydrophobic and superhydrophobic convex surfaces in a stationary situation. In this study, the reflection or deflection (teapot effect) of the liquid jet impinging the convex surface is dominated by the capillary adhesion interaction between the superhydrophobic and hydrophilic surfaces. Bizjan *et al*. (2021) have experimentally investigated the flow behavior of a liquid jet impinging on a rotating cylindrical surface at different jet velocities, cylinder rotation speeds, and impingement positions. They stated that the critical Reynolds number for splash onset was approximately the same as on a flat surface, but the splash onset increased substantially with increased jet impingement angle. Jambon-Puillet *et al*. (2019) have experimentally investigated the adhesion of a water jet to vertical cylinders. They showed that the impinging jet formed a helical shape wrapped around the convex surface depending on the initial speed and geometry of the jet.

In the present study, the behavior of the liquid jet impinging the moving superhydrophobic and hydrophilic surfaces is investigated. The impinging liquid jet on the superhydrophobic surfaces is examined, and the hydrophilic surface is studied for differences before and after impingement. For this purpose, rotating convex surfaces are used to obtain a constantly renewed interface between the liquid jet and the solid surface. The behavior of the liquid jet impinging on a stationary superhydrophobic surface has been studied many times before. However, liquid jets impinging on superhydrophobic surfaces in motion are far less well studied. The novelty of this study is the investigation of the conditions in which the liquid jet impinges on moving superhydrophobic surfaces and is almost unaffected by the motion of the surface. The effect of air film continuity between the superhydrophobic surface and the liquid is demonstrated and is due to a constantly renewed air film between the liquid and the solid.

2   EXPERIMENTAL SETUP

Figure 1a shows the experimental setup, consisting of two main components: a liquid jet and rotating systems. In the liquid jet system, distilled water (density, $\rho = 998$ kg/m^3; dynamic viscosity, $\mu = 0.96$ mPa.s; surface tension, $\gamma = 71.7$ mN/m) was pumped from a reservoir using a centrifugal pump. The 400 mm long straight, smooth glass tube, which had a 4 mm inner diameter, was used as a nozzle to generate the liquid jet. The flow rate of the jet was measured using a turbine-type flowmeter (McMillan S–114–7) in the range of 0.10–0.35 L/min. The flow rate of the liquid was precisely adjusted using a precision needle valve. The nozzle was held with a rotating clamp and the clamp was attached to the linear guide of a lathe (cross slide) using a magnetic base arm.

Precise horizontal movement of the nozzle was achieved in the x-direction by moving the cross slide with an accuracy of 0.02 mm on a vernier scale, as shown in Fig. 1b. In the rotating surface system, two copper pipes of 8 and 22 mm outer diameter, respectively, and a plexiglass pipe of 50 mm outer diameter were used as convex surfaces. These pipes were coated with a superhydrophobic coating (WX 2100), with an apparent contact angle of 157°. The uncoated plexiglass pipe had an apparent contact angle of 73°, which is considered hydrophilic. They were precisely connected horizontally to the rotating system.
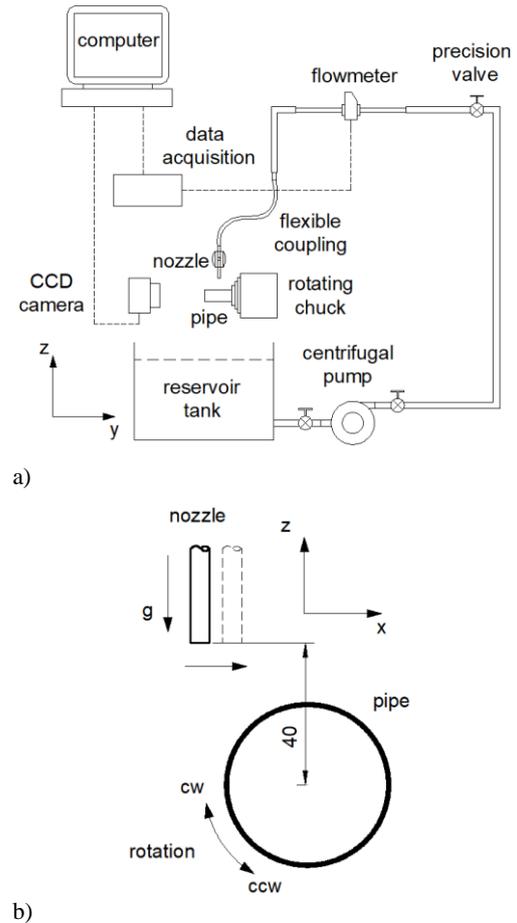

a)

b)

Fig. 1. Illustrations of a) experimental setup and b) nozzle translation, and pipe rotation.

2.1 Experimental Procedure

A lathe was used to rotate the pipes. These pipes were attached horizontally to the chucks of the lathe. The tip of the nozzle was placed 40 mm above the center of the cylinder, as shown in Fig. 1b. Initially, the flow rate of the liquid jet was set at the lowest rate (Re:1082 and We:3.90). The linear guide of the lathe carrying the nozzle was then moved in the x-direction until the edge of the liquid jet touched the pipe. When the liquid jet touched the pipe, the flow over the surface was recorded with a CCD camera from the side.

The nozzle was moved at impingement distance intervals of 0.4 mm in the x-direction, as shown in

Fig. 1b, to observe the effect of the impinging liquid jet on the convex surface. The experiment was continued using the same procedure as the impingement distance on the x-axis was increased, and the flow rate was varied. A total of 16 impingement distances (0, 0.4, 0.8,..., 6 mm) were tested. The same procedure was repeated while the cylinder rotated clockwise and counterclockwise at 125 rpm. The acquired data were recorded for evaluation. The Reynolds and Weber numbers were in the ranges 1082–3443 and 3.90–35.12, respectively. The impingement rate is obtained by dividing the impingement distance by the radius of the pipe, as defined by Kibar (2017). Therefore, the impingement rate ranged from 0 to 1.5 and 0 to 0.55 for the 8 and 22 mm outer diameter pipes, respectively.

The liquid jet flows vertically in the direction of gravity in the experiments, as shown in Fig. 2a. When the flow direction of the liquid jet was away from the surface, this type of flow was called reflection (Fig. 2b), and when the liquid jet followed the curve of the surface, it was called deflection (Fig. 2c). The angle of reflection was the angle between the liquid jet and the vertical direction, as shown in Fig. 2b.
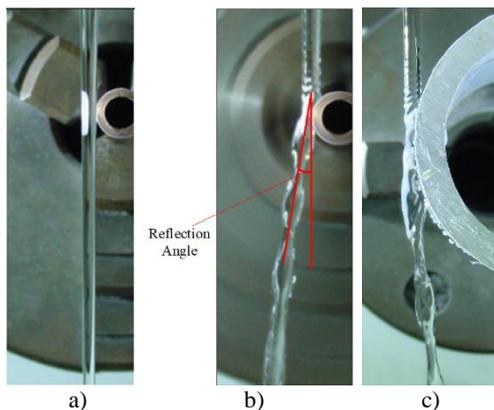

Fig. 2. Flow phenomena: a) Undisturbed, b) reflected, and c) deflected flows.

3   RESULTS AND DISCUSSION

Figure 3 shows the impingement of the liquid jets on the superhydrophobic convex surface at separate impingement rates from 0 to 0.55. The liquid jet impinging on the stationary superhydrophobic convex surface at a small impingement rate (0.036) reflects from the surface at a low angle since the surface energy of the jet is small due to the slight increase in the surface area of the spreading liquid (Kibar 2017), as shown in the first image in Fig. 3a. This reflection angle increases with increased impingement rate because of the increased stored surface energy, which is mostly affected by the difference between the free surface (liquid-air interface) and the wetted area (Kibar 2018a). When the impinging liquid jet spreads over the convex surface, the vertical momentum of the jet is converted into tangential momentum (and hence centrifugal force), and the liquid jet is reflected from

the surface by this tangential momentum (Kibar 2017). The contact angle, which is a result of the free surface energy of the solid surface, is the most effective parameter to describe the increase in the free surface area. Thus, due to the low free surface energy of the superhydrophobic surface, the free surface energy of the liquid is much higher than that of the wetting surface, resulting in the large stored surface energy of the spreading liquid (Kibar 2017).
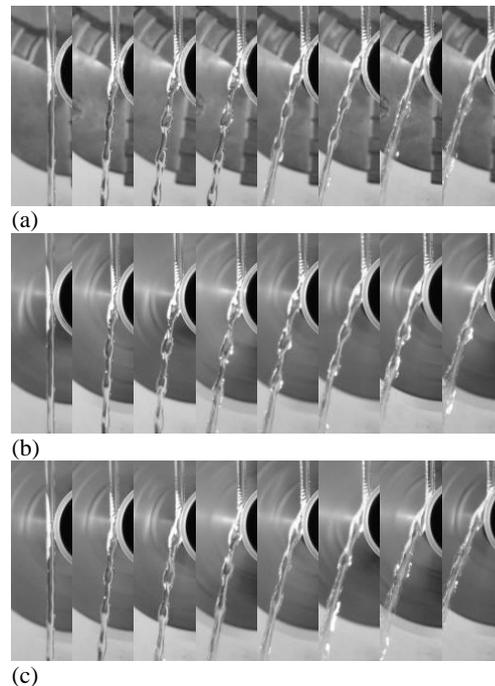

Fig. 3. Impingement of the liquid jet on the pipe a) stationary, b) rotating clockwise, and c) rotating counterclockwise. Pipe diameter: 22 mm, Re: 2702, We: 24.39. Note: There was an interval of approximately 5 seconds between the stationary, clockwise, and counterclockwise rotations in the experiments.

When the liquid jet impinges on a convex rotating superhydrophobic surface at a low impingement rate, the jet reflects off the surface at the same angle as a stationary surface, as shown in the first several images in Figs. 3b and 3c. The increase in the impingement rate barely affects the spreading and reflection phenomena of the liquid jet. As seen in the last two pictures in Figs. 3b and 3c, when the impingement rate is larger than ~0.5 the entire jet of liquid spreads over the surface, and the reflection angle of the jet is slightly affected by the rotation of the superhydrophobic surface. The air formed by the air pockets trapped in the micro/nano cavities on the superhydrophobic surface becomes a continuous air film with the rotating surface. Therefore, the liquid jet flows over the air film, which has a low viscosity compared to the liquid, by contacting at a few points on the surface. Therefore, the stored surface energy, which is the most important parameter for reflecting the liquid jet from the surface, is almost unaffected by the rotation of the superhydrophobic surface. When Figs. 3b and 3c are compared, the rotation direction of the pipe does not affect the reflection of

the liquid jet (under the experimental conditions in this study) very much. The direction of the movement of the surface does not make a significant difference to the flow of the liquid jet.

Figure 4 shows the behavior of liquid jet impingement on a superhydrophobic convex surface with a small diameter (8 mm) at the same impingement rate but with different Reynolds and Weber numbers. The lower Reynolds number jets are slightly more affected by the surface rotation than the higher values, as shown in Fig. 4. This effect is more pronounced when the direction of flow of the liquid jet and the direction of rotation of the superhydrophobic convex surface is different, as seen in Figs. 4a and 4b. In the jets with high Reynolds and Weber numbers (Fig. 4b), the effect of the vertical momentum dominates the stored surface energy of the spreading liquid on the convex surface. Therefore, it is less affected by the rotation of the convex surface. While the low Reynolds number jet has a low momentum, the low diameter convex surface has a high centrifugal force. This high centrifugal force creates a greater distortion effect on the flow of the liquid in contact with the superhydrophobic convex surface.
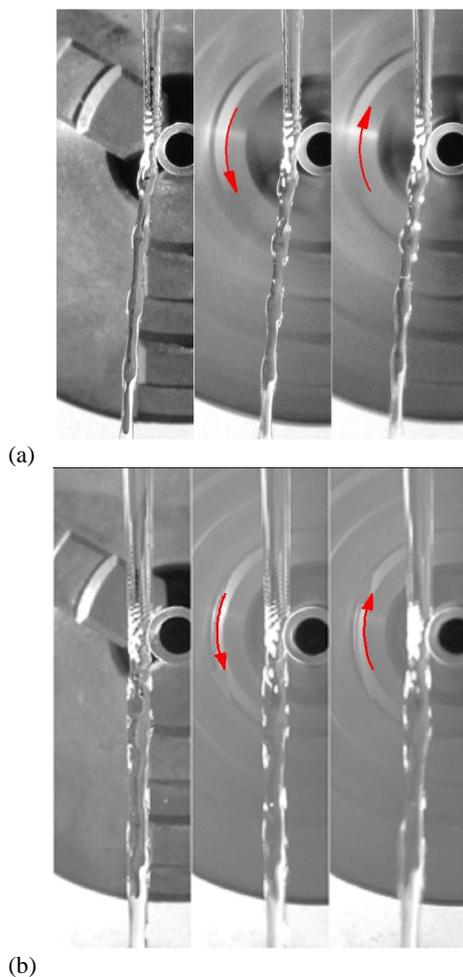

(a)

(b)

Fig. 4: Stationary, 125 rpm rotation in counterclockwise and 125 rpm rotation clockwise, a) Re:1081, We: 3.90, b) Re: 2702, We: 24.39. Pipe diameter: 8 mm, impingement rate: 0.3.

Figure 5 shows the impingement of a liquid jet that has the smallest Reynolds and Weber numbers in this study (Re: 1082, We: 3.90) on a rotating superhydrophobic convex surface 8 mm in diameter. On a stationary pipe, the reflection angle increases as the impingement rate increases. In the case of small impingement rates (≤ 0.5), the liquid jet impinging on the stationary and pipes rotating clockwise shows approximately the same reflection behavior. Alternatively, the reflection angles are slightly larger in the liquid jet hitting the pipe rotating counterclockwise, which is opposite to the flow direction of the liquid jet. As the impingement rate increases, the differences between the reflection angles in the stationary, clockwise, and counterclockwise cases also increase.

The liquid jet impinging on the 8 mm convex surface causes a higher centrifugal force than the 22 mm surface. This centrifugal force increases as the liquid jet velocity increases. As the liquid jet velocity increases, the centrifugal force increases even more since the centrifugal force is in direct proportion to the square of the velocity. The dominant parameter in the angle of reflection is the stored surface energy of the spreading jet on the convex surface. As the impingement rate increases, the stored surface energy of the liquid jet, which spreads over more of the surface, decreases. The magnitude of the stored surface energy is determined by the impingement rate, surface curvature, impingement velocity (Re or We), the velocity of the convex surface, and the contact angle with the surface.
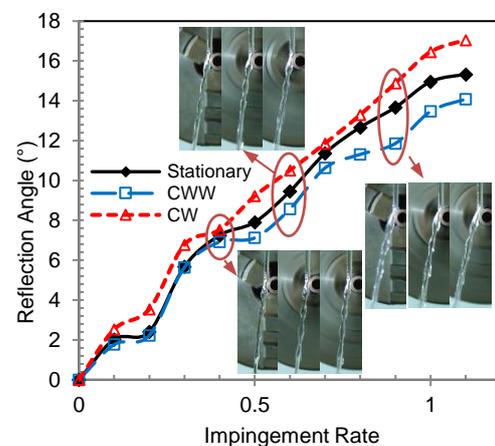

Fig. 5. Reflection angle of the liquid jet on the 8 mm diameter superhydrophobic pipe. Re: 1082, We: 3.90. Insets show data bounded by ellipses.

Figure 6 shows the impingement of the liquid jet on a horizontal superhydrophobic pipe, which has an outer diameter of 8 mm. The jet impinging on the center of the stationary pipe flows by dividing into two equal branches flowing sideways, as shown in Fig. 6a. The flows for both stationary and rotating pipes are almost the same. The flow phenomenon is not affected by the direction of the rotation of the pipe, as seen in Figs. 6b and 6c. There is an air film between the spreading liquid and the Cassie-Baxter-type superhydrophobic surface. The rotation of the

pipe constantly renews this film. Thus, the surface is prevented from moving into a Wenzel state because the air film does not disappear. Therefore, the liquid jet flows for a long time by contacting the surface in a few places. In this case, the inertia momentum of the liquid jet is more dominant than the capillary adhesion forces.
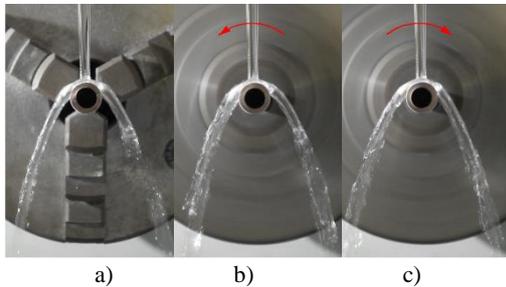

a)　　　　　　b)　　　　　　c)

Fig. 6. Impingement of the liquid jet on a superhydrophobic pipe with an outer diameter of 8 mm. a) Stationary b) Rotating counterclockwise at 125 rpm c) Rotating clockwise at 125 rpm, Re: 1891, We: 11.95.

Figure 7 shows the flow of the liquid jet hitting the center of the horizontal stationary pipe at higher Reynolds and Weber numbers compared to those in Fig. 6. The jet hitting the surface flows sideways by dividing into two equal branches, for both low and high Reynolds and Weber numbers, as shown in Figs. 6a and 7a, respectively. However, when the liquid jet with high Reynolds and Weber numbers impinges a rotating pipe, the flows divided into two branches are affected by the rotation of the pipe, as shown in Figs. 7b and 7c. While the reflection angle of the branch of the liquid jet on the opposite side of the pipe from the jet does not change significantly, the angle of reflection of the branch in the direction of rotation changes significantly. In the branch where the flow direction of the liquid jet and the rotation direction of the pipe are the same, the reflection angle is greatly reduced (left branch in Fig. 7b and right branch in Fig. 7c). Therefore, the angle between the two arms in the stationary and rotating pipes is reduced by approximately half. The impinging jet with high Reynolds and Weber numbers spreads over a large area, resulting in a much more complex flow. It is speculated that the increase in the jet velocity reduces the thickness of the air layer between the liquid and the surface in the region of jet impingement. Thus, the skin friction between the surface and the liquid increases. As the velocity of the liquid jet increases, the velocity of the liquid becomes much larger than the line velocity of the surface. In this way, since the wetting rate is greater than the spreading rate, the spreading liquid wrapped more closely to the surface (Duez *et al*. 2007).

When the liquid jet hits on a large diameter (50 mm) superhydrophobic convex surface, it reflects from the surface, as shown in Fig. 8a. The liquid jet gets almost the same event without being affected by forces such as drag resistance and the centrifugal forces that occur with the rotation of the surface, as shown in Fig. 8b. A liquid jet impinging a hydrophilic convex surface undergoes deflection
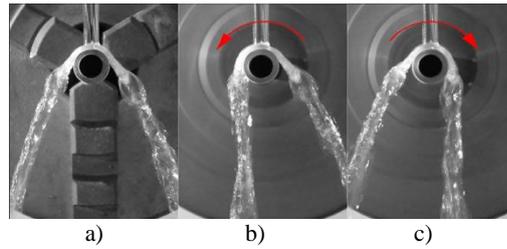

a)　　　　　　b)　　　　　　c)

Fig. 7. Impingement of the liquid jet on the 8 mm outer diameter superhydrophobic pipe. a) Stationary b) Rotating counterclockwise at 125 rpm c) Rotating clockwise at 125 rpm. Re: 3443, We: 35.12.
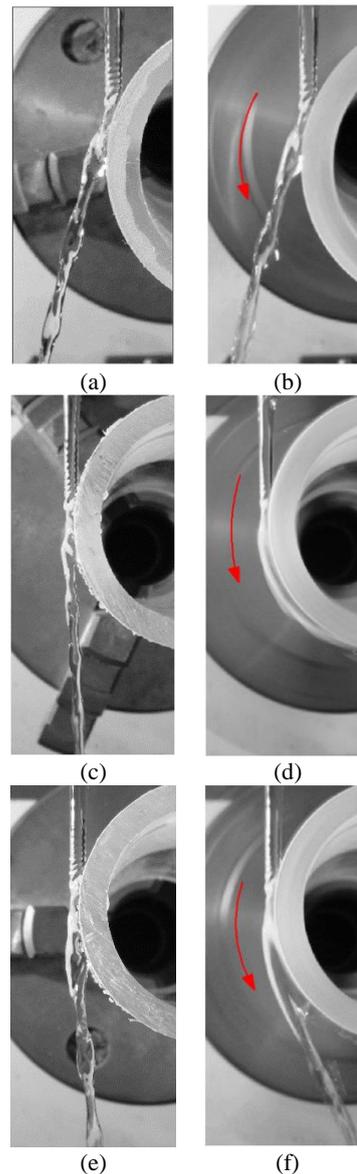

(a)　　　　　　(b)

(c)　　　　　　(d)

(e)　　　　　　(f)

Fig. 8. Liquid jet impinging on a) stationary superhydrophobic surface b) rotating superhydrophobic surface (Re:2702, We:24.39), c) stationary hydrophilic surface, d) rotating hydrophilic surface (Re:1082, We:3.90), e) stationary hydrophilic surface, and f) rotating hydrophilic surface (Re:2162, We:15.61). Pipe diameter: 50 mm.

instead of a reflection from the surface (Fig. 8c). This deflection occurs at a low rate because the contact angle of this surface is close to 90°, which is the hydrophobic limit. The liquid jet impinging the surface spreads over a wide area on the hydrophilic surface. In this case, the ratio between the free surface area of the spreading liquid and the wetting area is low. Thus, the liquid cannot obtain the energy to reflect from the surface since the stored surface energy is low (Kibar 2017). Furthermore, the wetting rate of the hydrophobic surface is greater than that of the superhydrophobic surface. Thus, the capillary adhesion force dominates the inertial momentum of the fluid jet. When the hydrophilic convex surface is rotated, the liquid jet is dragged by the surface; thus, it continues to flow, rotating with the surface, as shown in Fig. 8d. In this case, the liquid jet has low momentum. Therefore, the drag force dominates the flow compared to the momentum of the flow. When the momentum of the liquid jet is increased, it is dragged by the surface at a low rate, as shown in Figs. 8e and 8f.

4 CONCLUSIONS

This study experimentally investigates the impingement of a liquid jet on stationary and rotating superhydrophobic and hydrophilic convex surfaces. On a hydrophilic surface, the liquid jet is in contact with the surface over a large area. Thus, the liquid jet impinging the moving surface is dragged by the surface, resulting in deflection. However, an impinging liquid jet on a superhydrophobic surface reflects off the surface. Furthermore, the reflection phenomenon of the liquid jet is largely unaffected by the motion of the superhydrophobic surface.

The most important parameter in the behavior of the liquid jet impinging the superhydrophobic surface is the contact angle. Air pockets between the liquid and the surface also affect the formation of the contact angle. Thanks to these air pockets, the contact area between the liquid jet and the surface is low compared to the free surface of the liquid, resulting in large stored surface energy. Therefore, the momentum of the liquid jet hitting a moving surface is greater than the drag force applied by the surface to the liquid jet. In this way, the liquid jet is unaffected by the movement of the surface.

Experimental, theoretical, and numerical studies can be conducted to improve this study, using variables such as the pipe diameter, liquid jet diameter, Reynolds and Weber Numbers, impingement rate, impingement angle of the liquid jet, the rotation speed of the convex surface, and the contact angle of the surface. The effect of the differences between the velocity of the liquid jet and the linear velocity of the cylinder surface can be examined on the liquid jet spreading and reflection behavior by using different cylinder rotational speeds.

REFERENCES

Abdelaziz, A. and R. E. Khayat (2022). On the non-circular hydraulic jump for an impinging inclined jet. *Physics of Fluids* 34(2), 023603.

Bhushan, B. and Y. C. Jung (2011). Natural and biomimetic artificial surfaces for superhydrophobicity, self-cleaning, low adhesion, and drag reduction. *Progress in Materials Science* 56(1), 1–108.

Bizjan, B., B. Širok and M. Blagojevič (2021). Free surface lubrication of rotating cylinders by impacting Newtonian liquid jet. *Lubrication Science* 33(8), 439–449.

Blake, T. D. (2006). The physics of moving wetting lines. *Journal of Colloid and Interface Science* 299(1), 1–13.

Cardin, K., S. Wang, O. Desjardins and M. Weislogel (2021). Rebound of large jets from superhydrophobic surfaces in low gravity. *Physical Review Fluids* 6(1), 014003.

Chatterjee, N. and M. Flury (2013). Effect of particle shape on capillary forces acting on particles at the air-water interface. *Langmuir* 29(25), 7903–7911.

Craik, A. D. D., R. C. Latham, M. J. Fawkes and P. W. F. Gribbon (1981). The circular hydraulic jump. *Journal of Fluid Mechanics* 112, 347–362.

de la Cruz, R. M. and S. A. Mäkiharju (2022). Jet impingement on the underside of a superhydrophobic surface. *Journal of Fluid Mechanics* 938, A4.

Duez, C., C. Ybert, C. Clanet and L. Bocquet (2007). Making a splash with water repellency. *Nature Physics* 3(March), 180–183.

Eral, H. B., T. Mannetje, D. J. C. M. and J. M. Oh (2013). Contact angle hysteresis: A review of fundamentals and applications. Colloid and Polymer Science 291, 247–260.

Erbil, H. Y., A. L. Demirel, Y. Avci and O. Mert (2003). Transformation of a simple plastic into a superhydrophobic surface. *Science* 299(5611), 1377–1380.

Jambon-Puillet, E., W. Bouwhuis, J. H.Snoeijer and D. Bonn (2019). Liquid Helix: How Capillary Jets Adhere to Vertical Cylinders. *Physical Review Letters* 122(18), 184501.

Kate, R. P., P. K. Das and S. Chakraborty (2007). Hydraulic jumps due to oblique impingement of circular liquid jets on a flat horizontal surface. *Journal of Fluid Mechanics* 573, 247–263.

Kibar, A. (2016). Experimental and numerical investigations of the impingement of an oblique liquid jet onto a superhydrophobic surface: energy transformation. *Fluid Dynamics Research* 48(1), 015501.

Kibar, A. (2017). Experimental and numerical investigation of liquid jet impingement on superhydrophobic and hydrophobic convex surfaces. *Fluid Dynamics Research* 49(1),

015502.

Kibar, A. (2018a). Experimental and numerical investigation on a liquid jet impinging on a vertical superhydrophobic surface: spreading and reflection. *Progress in Computational Fluid Dynamics, An International Journal* 18, 150-63.

Kibar, A. (2018b). The Spreadıng Profile Of An Impınging Lıquıd Jet On The Hydrophobıc Surfaces. *Sigma Journal of Engineering and Natural Sciences* 36(3), 609–618.

Kibar, A., H. Karabay, K. S. Yiğit, I. O. Ucar and H. Y. Erbil (2010). Experimental investigation of inclined liquid water jet flow onto vertically located superhydrophobic surfaces. *Experiments in Fluids* 49, 1135–1145.

Landel, J. R. and D. I. Wilson (2021). The Fluid Mechanics of Cleaning and Decontamination of Surfaces. In *Annual Review of Fluid Mechanics* 53, 147-171.

Latthe, S. S., R. S. Sutar, V. S. Kodag, A. K. Bhosale A. M.Kumar, K. Kumar Sadasivuni, R. Xing and S. Liu (2019). Self – cleaning superhydrophobic coatings: Potential industrial applications. *Progress in Organic Coatings* 128, 52–58.

Li, P., L. Yang and Q. Fu (2021). Effect of surface contact angle on the wall impingement of a power-law liquid jet. *Physics of Fluids 33*(4) 043105.

Linder, N., A. Criscione, I. V. Roisman, H. Marschall and C. Tropea (2015). 3D computation of an incipient motion of a sessile drop on a rigid surface with contact angle hysteresis. *Theoretical and Computational Fluid Dynamics* 29(5–6), 373–390.

Lu, Q., R. Muthukumar, H. Ge and S. Parameswaran (2020). Numerical study of a rotating liquid jet impingement cooling system. *International Journal of Heat and Mass Transfer* 163, 120446.

Mertens, K., V. Putkaradze and P. Vorobieff (2005). Morphology of a stream flowing down an inclined plane. Part 1. Braiding. *Journal of Fluid Mechanics* 531, 49–58.

Prince, J. F., D. Maynes and J. Crockett (2015). On jet impingement and thin film breakup on a horizontal superhydrophobic surface. *Physics of Fluids* 27(11), 112108.

Satpathi, N. S., L. Malik, A. S. Ramasamy and A. K. Sen (2021). Drop impact on a superhydrophilic spot surrounded by a superhydrophobic surface. *Langmuir* 37(48), 14195–14204.

Sen, U., S. Chatterjee, J. Crockett, R. Ganguly, L. Yu and C. M. Megaridis (2019). Orthogonal liquid-jet impingement on wettability-patterned impermeable substrates. *Physical Review Fluids* 4(1), 014002.

Shi, L., Y. Li, Y. Meng, G. Hu and Y. Tian (2018). Fluid Property Effects on the Splashing in Teapot Effect. *The Journal of Physical Chemistry C* 122(37), 21411–21417.

Varshney, P. and S. S. Mohapatra (2018). Durable and regenerable superhydrophobic coatings for brass surfaces with excellent self-cleaning and anti-fogging properties prepared by immersion technique. *Tribology International* 123, 17–25.

Wu, Y., Y. Shen, J. Tao, Z. He, Y. Xie, H. Chen, M. Jin and W. Hou (2018). Facile spraying fabrication of highly flexible and mechanically robust superhydrophobic F-SiO2@PDMS coatings for self-cleaning and drag-reduction applications. *New Journal of Chemistry* 42(22), 18208–18216.

Yang, L. J., P. H. Li and Q. F. Fu (2020). Liquid sheet formed by a Newtonian jet obliquely impinging on pro/hydrophobic surfaces. *International Journal of Multiphase Flow* 125, 103192.

Yao, X., W. Jiang, J. Yang, J. Fang and W. Zhang (2021). A Surface Energy Approach to Developing an Analytical Model for the Underfill Flow Process in Flip-Chip Packaging. *Journal of Electronic Packaging*, 144(4), 041003.

Zhang, L., J. Wu, M. N. Hedhili, X. Yang and P. Wang (2015). Inkjet printing for direct micropatterning of a superhydrophobic surface: Toward biomimetic fog harvesting surfaces. *Journal of Materials Chemistry A* . 3(6), 2844-2852.